Supplementary Information

Positive feedback loops for factor V and factor VII activation supply sensitivity to local surface tissue factor density during blood coagulation

A.N. Balandina[1,2], A.M. Shibeko[2], D.A. Kireev[2], A.A. Novikova[1], I.I. Shmirev[2], M.A. Panteleev[1,2], F. I. Ataullakhanov[1,2,3]

[1] Center for Theoretical Problems of Physicochemical Pharmacology, Moscow 119991, Russia

[2] National Research Center for Hematology, Moscow 125167, Russia

[3] Department of Physics, Moscow State University, Moscow 119991, Russia

Table of contents

1. Model description

1.1. Model assumptions and modification

The principal model assumptions and their substantiation can be found in (1). Initial concentrations are listed in Table S1. Reaction constants are listed in Tables S2 and S3. For purposes of this study, the model was modified as follows: a) thrombomodulin was removed, as it was absent in the experimental system studied; b) three spatial dimensions and 3D diffusion were introduced; and c) several kinetic constants in the model were changed to conform to the experimental conditions (see Table S2). To make the model equations simpler, we removed platelets and their activation because all experiments in the study herein were performed in platelet-free plasma. Therefore, membrane binding sites for intrinsic tenase, prothrombinase, and other membrane-binding complexes/proteins are in the platelet-derived microparticles and plasma lipoproteins. All reactions catalyzed by intrinsic tenase, prothrombinase, and others explicitly included the concentration of the binding sites. The procoagulant activity of platelet-derived microparticles and lipoproteins in platelet-free plasma (expressed as the number of binding sites) was estimated in the model using experimental reports as described in (1). Because these values were reported, the validity of such estimations was also confirmed by our studies on spatial fibrin clot formation in ultra-centrifuged plasma that was titrated with either platelets, activated platelets, or platelet-derived microparticles (1,2).

1.2. Model equations

Notation. The concentration of a factor F is denoted as [*F*]. All model variables represent the total concentrations; for example, [*IXa*] is the concentration of total IXa, including fIXa free in solution, in complex with fVIIIa, and in the enzyme-substrate complex with fX. The concentration of free factor F in solution is $[F^F]$; for most factors, $[F^F]$~[*F*]. The concentration of factor F bound to activated platelets is denoted $[F^B]$; $\left\lfloor F^{B\,F} \right\rfloor$ is factor F bound to activated platelets, but free and not in complex with other factors at the platelet membrane. An exception to this notation is $\left\lfloor Va^{B\,F} \right\rfloor$, which represents fVa bound to both intact and activated platelets and susceptible to inactivation by APC.

Rate constants for F_1 and F_2 association and dissociation are $k_a^{F_1,F_2}$ and $k_d^{F_1,F_2}$, respectively; the equilibrium dissociation constant is designated $K_d^{F_1,F_2}$. The subscript i identifies a competitive inhibition constant. K_d^F and n^F are the equilibrium dissociation constant and the number of binding

sites per platelet, respectively, for factor F. Constants $k_{cat}^{F_1,F_2}$, $K_M^{F_1,F_2}$, and $k_{eff}^{F_1,F_2}$ are the catalytic, Michaelis and effective rate constants, respectively, for factor F_1 catalysis by enzyme F_2. The superscript "local" indicates an intrinsic, two-dimensional constant for reactions at the activated platelet membrane. The symbol *k* in the denominator for local constants is the parameter used to link them to 3D concentrations (3). The symbol ρ^F represents the number of factor F molecules secreted per platelet upon activation. Surface densities for the factors on the activating surface are designated σ; for example, σ_{TF} is the TF surface density. The diffusion coefficient for factor F is denoted D_F.

Equations:

1. Initiation:

$$\frac{d\sigma_{VIIa-TF}}{dt} = \left(k_a^{VIIa,TF} \cdot [VIIa]_{x=0} \cdot \sigma_{TF} - k_d^{VIIa-TF} \cdot {\sigma_{VIIa-TF}}^F\right) + \frac{k_{cat}^{VII-TF,IIa} \cdot \sigma_{VII-TF} \cdot [IIa^F]_{x=0}}{K_M^{VII-TF,IIa} + [IIa^F]_{x=0}} +$$

$$+ k_{eff}^{VII-TF,Xa} \cdot \sigma_{VII-TF} \cdot [Xa^F]_{x=0} -$$

$$- k_a^{VIIa-TF,Xa-TFPI} \cdot [Xa-TFPI]_{x=0} \cdot {\sigma_{VIIa-TF}}^F - k_a^{Xa-VIIa-TF,TFPI} \cdot \sigma_{Xa-VIIa-TF} \cdot [TFPI]_{x=0} \quad \text{(S1)}$$

$$\frac{d\sigma_{VII-TF}}{dt} = \left(k_a^{VII,TF} \cdot [VII]_{x=0} \cdot \sigma_{TF} - k_d^{VII-TF} \cdot \sigma_{VII-TF}\right) - \frac{k_{cat}^{VII-TF,IIa} \cdot \sigma_{VII-TF} \cdot [IIa^F]_{x=0}}{K_M^{VII-TF,IIa} + [IIa^F]_{x=0}} -$$

$$- k_{eff}^{VII-TF,Xa} \cdot \sigma_{VII-TF} \cdot [Xa^F]_{x=0}$$

$$\frac{d\sigma_{TF}}{dt} = -\left(k_a^{VIIa,TF} \cdot [VIIa]_{x=0} \cdot \sigma_{TF} - k_d^{VIIa-TF} \cdot {\sigma_{VIIa-TF}}^F\right) - \quad \text{(S3)}$$

$$- \left(k_a^{VII,TF} \cdot [VII]_{x=0} \cdot \sigma_{TF} - k_d^{VII-TF} \cdot \sigma_{VII-TF}\right)$$

$$\frac{\partial[VIIa]}{\partial t} = D_{VIIa} \cdot \left(\frac{\partial^2[VIIa]}{\partial x^2} + \frac{\partial^2[VIIa]}{\partial y^2} + \frac{\partial^2[VIIa]}{\partial z^2}\right) + \frac{k_{cat}^{VII,IIa} \cdot [VII] \cdot [IIa^F]}{K_M^{VII,IIa} + [IIa^F]} \quad \text{(S4)}$$

$$\frac{\partial[VII]}{\partial t} = D_{VII} \cdot \left(\frac{\partial^2[VII]}{\partial x^2} + \frac{\partial^2[VII]}{\partial y^2} + \frac{\partial^2[VII]}{\partial z^2}\right) - \frac{k_{cat}^{VII,IIa} \cdot [VII] \cdot [IIa^F]}{K_M^{VII,IIa} + [IIa^F]} \quad \text{(S5)}$$

2. Cascade backbone:

$$\frac{\partial[IXa]}{\partial t} = D_{IXa} \cdot \left(\frac{\partial^2[IXa]}{\partial x^2} + \frac{\partial^2[IXa]}{\partial e^2} + \frac{\partial^2[IXa]}{\partial z^2}\right) + k_{contact} \cdot [IX] +$$

$$+ \frac{k_{cat}^{IX,XIa} \cdot [IX] \cdot [XIa]}{K_M^{IX,XIa} + [IX]} - k_a^{IXa,AT-III} \cdot [AT-III] \cdot [IXa] \quad \text{(S6)}$$

$$\frac{\partial[IX]}{\partial t} = D_{IX} \cdot \left(\frac{\partial^2[IX]}{\partial x^2} + \frac{\partial^2[IX]}{\partial y^2} + \frac{\partial^2[IX]}{\partial z^2}\right) - k_{contact} \cdot [IX] - \frac{k_{cat}^{IX,XIa} \cdot [IX] \cdot [XIa]}{K_M^{IX,XIa} + [IX]} \tag{S7}$$

$$\frac{\partial[Xa]}{\partial t} = D_{Xa} \cdot \left(\frac{\partial^2[Xa^F]}{\partial x^2} + \frac{\partial^2[Xa^F]}{\partial y^2} + \frac{\partial^2[Xa^F]}{\partial z^2}\right) +$$

$$+ \frac{k_{cat}^{X,IXa\,local} \cdot [IXa^{BF}] \cdot [X^B]}{N_a \cdot K_M^{X,IXa\,local}/k} + \frac{k_{cat}^{X,IXa-VIIIa\,local} \cdot [IXa^{BF}] \cdot [VIIIa^{BF}] \cdot [X^B]}{N_a \cdot K_d^{IXa-VIIIa\,local}/k \cdot N_a \cdot K_M^{X,IXa-VIIIa\,local}/k} - \tag{S8}$$

$$- \left(k_a^{Xa,AT-III} \cdot [AT-III] + k_a^{Xa,\alpha_2 M} \cdot [\alpha_2 M]_0 + k_a^{Xa,\alpha_1 AT} \cdot [\alpha_1 AT]_0 + k_a^{Xa,PCI} \cdot [PCI]_0\right) \cdot [Xa^F] -$$

$$- k_a^{Xa-Va^B,AT-III} \cdot [AT-III] \cdot [Xa-Va^B] -$$

$$- \left(k_a^{Xa,TFPI} \cdot [Xa^F] \cdot [TFPI] - k_d^{Xa-TFPI} \cdot [Xa-TFPI]\right)$$

$$\frac{\partial[X]}{\partial t} = D_X \cdot \left(\frac{\partial^2[X]}{\partial x^2} + \frac{\partial^2[X]}{\partial y^2} + \frac{\partial^2[X]}{\partial z^2}\right) - \tag{S9}$$

$$- \frac{k_{cat}^{X,IXa\,local} \cdot [IXa^{BF}] \cdot [X^B]}{N_a \cdot K_M^{X,IXa\,local}/k} - \frac{k_{cat}^{X,IXa-VIIIa\,local} \cdot [IXa^{BF}] \cdot [VIIIa^{BF}] \cdot [X^B]}{N_a \cdot K_d^{IXa-VIIIa\,local}/k \cdot N_a \cdot K_M^{X,IXa-VIIIa\,local}/k}$$

$$\frac{\partial[IIa]}{\partial t} = D_{IIa} \cdot \left(\frac{\partial^2[IIa^F]}{\partial x^2} + \frac{\partial^2[IIa^F]}{\partial y^2} + \frac{\partial^2[IIa^F]}{\partial z^2}\right) + k_{eff}^{II,Xa} \cdot N_a \cdot [Xa^F] \cdot [II] + \tag{S10}$$

$$\frac{k_{cat}^{local\,II,Xa-Va} \cdot [Xa-Va^B] \cdot [II^B]}{K_M^{local\,II,Xa-Va}/k \cdot N_a} -$$

$$- \left(k_a^{IIa,AT-III} \cdot [AT-III] + k_a^{IIa,\alpha_2 M} \cdot [\alpha_2 M]_0 + k_a^{IIa,\alpha_1 AT} \cdot [\alpha_1 AT]_0 + k_a^{IIa,PCI} \cdot [PCI]_0 + k_a^{IIa,HC-II} \cdot [HC-II]_0\right) \cdot [IIa^F]$$

$$\frac{\partial[II]}{\partial t} = D_{II} \cdot \left(\frac{\partial^2[II]}{\partial x^2} + \frac{\partial^2[II]}{\partial y^2} + \frac{\partial^2[II]}{\partial z^2}\right) - k_{eff}^{II,Xa} \cdot N_a \cdot [Xa^F] \cdot [II] - \frac{k_{cat}^{local\,II,Xa-Va} \cdot [Xa-Va^B] \cdot [II^B]}{K_M^{local\,II,Xa-Va}/k \cdot N_a} \tag{S11}$$

$$\frac{\partial[Fn]}{\partial t} = \frac{k_{cat}^{Fg,IIa} \cdot [Fg] \cdot [IIa^F]}{K_M^{Fg,IIa}} \tag{S12}$$

$$\frac{\partial[Fg]}{\partial t} = D_{Fg} \cdot \left(\frac{\partial^2[Fg]}{\partial x^2} + \frac{\partial^2[Fg]}{\partial y^2} + \frac{\partial^2[Fg]}{\partial z^2}\right) - \frac{k_{cat}^{Fg,IIa} \cdot [Fg] \cdot [IIa^F]}{K_M^{Fg,IIa}} \tag{S13}$$

3. Cofactor activation:

$$\frac{\partial[VIIIa]}{\partial t} = D_{VIIIa} \cdot \left(\frac{\partial^2[VIIIa]}{\partial x^2} + \frac{\partial^2[VIIIa]}{\partial y^2} + \frac{\partial^2[VIIIa]}{\partial z^2}\right) + \frac{k_{cat}^{VIII,IIa} \cdot [VIII] \cdot [IIa^F]}{K_M^{VIII,IIa} + [IIa^F]} - h^{VIIIa} \cdot [VIIIa] \tag{S14}$$

$$\frac{\partial[VIII]}{\partial t} = - \frac{k_{cat}^{VIII,IIa} \cdot [VIII] \cdot [IIa^F]}{K_M^{VIII,IIa} + [IIa^F]} \tag{S15}$$

$$\frac{\partial[Va]}{\partial t} = D_{Va} \cdot \left(\frac{\partial^2[Va]}{\partial x^2} + \frac{\partial^2[Va]}{\partial y^2} + \frac{\partial^2[Va]}{\partial z^2}\right) + \frac{k_{cat}^{V,IIa} \cdot [V] \cdot [IIa^F]}{K_M^{V,IIa} + [IIa^F]} - k_{eff}^{local\,Va,APC} \cdot [APC] \cdot [Va^{BF}] \quad \text{(S16)}$$

$$\frac{\partial[V]}{\partial t} = D_V \cdot \left(\frac{\partial^2[V]}{\partial x^2} + \frac{\partial^2[V]}{\partial y^2} + \frac{\partial^2[V]}{\partial z^2}\right) - \frac{k_{cat}^{V,IIa} \cdot [V] \cdot [IIa^F]}{K_M^{V,IIa} + [IIa^F]} \quad \text{(S17)}$$

4. Inhibition:

$$\frac{\partial[APC]}{\partial t} = D_{PCa} \cdot \left(\frac{\partial^2[APC]}{\partial x^2} + \frac{\partial^2[APC]}{\partial y^2} + \frac{\partial^2[APC]}{\partial z^2}\right) + \frac{k_{cat}^{PC,IIa} \cdot [PC] \cdot [IIa^F]}{K_M^{PC,IIa}} +$$

$$+ k_{eff}^{PC,APC} \cdot [PC] \cdot [APC] - \quad \text{(S18)}$$

$$- \left(k_a^{APC,\alpha_2 M} \cdot [\alpha_2 M]_0 + k_a^{APC,\alpha_2 AP} \cdot [\alpha_2 AP]_0 + k_a^{APC,\alpha_1 AT} \cdot [\alpha_1 AT]_0 + k_a^{APC,PCI} \cdot [PCI]_0\right) \cdot [APC]$$

$$\frac{\partial[PC]}{\partial t} = D_{PC} \cdot \left(\frac{\partial^2[PC]}{\partial x^2} + \frac{\partial^2[PC]}{\partial y^2} + \frac{\partial^2[PC]}{\partial z^2}\right) - \frac{k_{cat}^{PC,IIa} \cdot [PC] \cdot [IIa^F]}{K_M^{PC,IIa}} - \quad \text{(S19)}$$

$$- k_{eff}^{PC,APC} \cdot [PC] \cdot [APC]$$

$$\frac{\partial[Xa-TFPI]}{\partial t} = D_{Xa-TFPI} \cdot \left(\frac{\partial^2[Xa-TFPI]}{\partial x^2} + \frac{\partial^2[Xa-TFPI]}{\partial y^2} + \frac{\partial^2[Xa-TFPI]}{\partial z^2}\right) + \quad \text{(S20)}$$

$$\left(k_a^{Xa,TFPI} \cdot [Xa^F] \cdot [TFPI] - k_d^{Xa-TFPI} \cdot [Xa-TFPI]\right)$$

$$\frac{\partial[TFPI]}{\partial t} = D_{TFPI} \cdot \left(\frac{\partial^2[TFPI]}{\partial x^2} + \frac{\partial^2[TFPI]}{\partial y^2} + \frac{\partial^2[TFPI]}{\partial z^2}\right) - \quad \text{(S21)}$$

$$\left(k_a^{Xa,TFPI} \cdot [Xa^F] \cdot [TFPI] - k_d^{Xa-TFPI} \cdot [Xa-TFPI]\right)$$

$$\frac{\partial[AT-III]}{\partial t} = D_{AT-III} \cdot \left(\frac{\partial^2[AT-III]}{\partial x^2} + \frac{\partial^2[AT-III]}{\partial y^2} + \frac{\partial^2[AT-III]}{\partial z^2}\right) - k_a^{IXa,AT-III} \cdot [AT-III] \cdot [IXa] -$$

$$- k_a^{Xa,AT-III} \cdot [AT-III] \cdot [Xa^F] - k_a^{Xa-Va^B,AT-III} \cdot [AT-III] \cdot [Xa-Va^B] - \quad \text{(S22)}$$

$$- k_a^{IIa,AT-III} \cdot [AT-III] \cdot [IIa^F] - k_a^{XIa,AT-III} \cdot [AT-III] \cdot [XIa] - k_a^{IIa-sTm,AT-III} \cdot [AT-III] \cdot [IIa]$$

5. Long-range feedback:

$$\frac{\partial[XIa]}{\partial t} = D_{XIa} \cdot \left(\frac{\partial^2[XIa]}{\partial x^2} + \frac{\partial^2[XIa]}{\partial y^2} + \frac{\partial^2[XIa]}{\partial z^2}\right) + k_{eff}^{XI,IIa} \cdot N_a \cdot [XI] \cdot [IIa^F] - \quad \text{(S23)}$$

$$- \left(k_a^{XIa,AT-III} \cdot [AT-III] + k_a^{XIa,\alpha_2 AP} \cdot [\alpha_2 AP]_0 + k_a^{XIa,\alpha_1 AT} \cdot [\alpha_1 AT]_0 + k_a^{XIa,PCI} \cdot [PCI]_0 + k_a^{XIa,C1I} \cdot [C1I]_0\right) \cdot [XIa]$$

$$\frac{\partial[XI]}{\partial t} = D_{XI} \cdot \left(\frac{\partial^2[XI]}{\partial x^2} + \frac{\partial^2[XI]}{\partial y^2} + \frac{\partial^2[XI]}{\partial z^2}\right) - k_{eff}^{XI,IIa} \cdot N_a \cdot [XI] \cdot [IIa^F] \quad \text{(S24)}$$

6. The compact notation for free and bound factor and factor complex concentrations in sections 1-8, above, should be read as follows.

$$\sigma_{VIIa-TF}{}^{F} = \frac{\sigma_{VIIa-TF}}{1 + \frac{[IX]_{x=0}}{K_M^{IX,VIIa-TF}} + \frac{[X]_{x=0}}{K_M^{X,VIIa-TF}}} \tag{S26}$$

$$\sigma_{X-VIIa-TF} = \frac{[X]_{x=0} \cdot \sigma_{VIIa-TF}}{K_M^{X,VIIa-TF} \cdot \left(1 + \frac{[IX]_{x=0}}{K_M^{IX,VIIa-TF}} + \frac{[X]_{x=0}}{K_M^{X,VIIa-TF}}\right)} \tag{S27}$$

$$\sigma_{Xa-VIIa-TF} = \frac{k_{cat}^{X,VIIa-TF} \cdot \sigma_{X-VIIa-TF}}{k_d^{Xa-VIIa-TF}} \tag{S28}$$

$$[IXa^{BF}] = \frac{[IXa] \cdot N_a \cdot n^{IXa}}{K_d^{IXa} + [IXa]} \tag{S29}$$

$$[VIIIa^{BF}] = \frac{[VIIIa] \cdot N_a \cdot n^{VIIIa}}{\left(K_d^{VIIIa} + [VIIIa]\right) \cdot \left(1 + \frac{[X^B]}{N_a \cdot K_d^{VIIIa-X\,local}/k}\right)} \cdot \frac{1}{1 + \frac{PS}{K_i^{VIIIa,PS}}} \tag{S30}$$

$$[Xa\text{–}Va^{B}] = \frac{[Xa] \cdot [Va^{B}]}{K_d^{Xa-Va} \cdot \left(1 + \frac{[PS]}{K_i^{Va,PS}} + \frac{[Xa]}{K_d^{Xa-Va}}\right) + [Va^{B}]} \tag{S31}$$

$$[Xa^{F}] = [Xa] - [Xa\text{–}Va^{B}] \tag{S32}$$

$$[X^{B}] = \frac{[X] \cdot N_a \cdot n^{X(II)}}{K_d^{X} \cdot \left(1 + \frac{[X]}{K_d^{X}} + \frac{[II]}{K_d^{II}}\right)} \tag{S33}$$

$$[IIa^{F}] = \frac{[IIa]}{1 + \frac{[Fg] + [Fn]}{K_M^{Fg,IIa}}} \tag{S34}$$

$$[II^{B}] = \frac{[II] \cdot N_a \cdot n^{X(II)}}{K_d^{II} \cdot \left(1 + \frac{[X]}{K_d^{X}} + \frac{[II]}{K_d^{II}}\right)} \tag{S35}$$

$$[Va^{B}] = \frac{[Va] \cdot N_a \cdot n^{Va}}{K_d^{Va} + [Va]} \tag{S36}$$

$$[Va^{BF}] = \frac{[Va] \cdot N \cdot \tilde{n}^{Va}}{\tilde{K}_d^{Va} + [Va]} + \frac{[Va] \cdot N_a \cdot n^{Va}}{K_d^{Va} + [Va]} - [Xa\text{–}Va^{B}] \tag{S37}$$

7. Boundary conditions:

For most factors, non-permeability conditions were used for all simulated volume surfaces. An example is given for prothrombin:

$$D_{IIa}\cdot\left.\frac{\partial[II]}{\partial x}\right|_{\Omega}=D_{IIa}\cdot\left.\frac{\partial[II]}{\partial y}\right|_{\Delta}=D_{IIa}\cdot\left.\frac{\partial[II]}{\partial z}\right|_{\Psi,\Lambda}=0 \tag{S38}$$

where Ω,Δ,Ψ and Λ are:

$$\begin{cases}\Omega\in\{x=0\cup x=L_x, y\in[0,L_y], z\in[0,L_z]\}\\ \Delta\in\{x\in[0,L_x], y=0\cup y=L_y, z\in[0,L_z]\}\\ \Psi\in\{x\in[0,L_x], y\in[0,L_y], z=L_z\}\\ \Lambda\in\{x\in[0,L_x], y\in[0,L_y], z=0\}\end{cases} \tag{S39}$$

The exceptions were fIXa, fIX, fXa, fX, Xa-TFPI, and TFPI, as activation reactions at the left end of the simulated interval cause changes in the boundary conditions, which correspond to the "flow" of these factors across the boundary, due to either activation or binding.

$$D_{VIIa}\cdot\left.\frac{\partial[VIIa]}{\partial x}\right|_{\Lambda}=\left(k_a^{VIIa,TF}\cdot[VIIa]_{\Lambda}\cdot\sigma_{TF}-k_d^{VIIa-TF}\cdot{\sigma_{VIIa-TF}}^{F}\right) \tag{S40}$$

$$D_{VII}\cdot\left.\frac{\partial[VII]}{\partial x}\right|_{\Lambda}=\left(k_a^{VII,TF}\cdot[VII]_{\Lambda}\cdot\sigma_{TF}-k_d^{VII-TF}\cdot\sigma_{VII-TF}\right) \tag{S41}$$

$$D_{IXa}\cdot\left.\frac{\partial[IXa]}{\partial x}\right|_{\Lambda}=-\frac{k_{cat}^{IX,VIIa-TF}\cdot[IX]_{\Lambda}\cdot{\sigma_{VIIa-TF}}^{F}}{K_M^{IX,VIIa-TF}} \tag{S42}$$

$$D_{IX}\cdot\left.\frac{\partial[IX]}{\partial x}\right|_{\Lambda}=\frac{k_{cat}^{IX,VIIa-TF}\cdot[IX]_{\Lambda}\cdot{\sigma_{VIIa-TF}}^{F}}{K_M^{IX,VIIa-TF}} \tag{S43}$$

$$D_{Xa}\cdot\left.\frac{\partial[Xa^F]}{\partial x}\right|_{\Lambda}=-\frac{k_{cat}^{X,VIIa-TF}\cdot[X]_{\Lambda}\cdot{\sigma_{VIIa-TF}}^{F}}{K_M^{X,VIIa-TF}} \tag{S44}$$

$$D_{X}\cdot\left.\frac{\partial[X]}{\partial x}\right|_{\Lambda}=\frac{k_{cat}^{X,VIIa-TF}\cdot[X]_{\Lambda}\cdot{\sigma_{VIIa-TF}}^{F}}{K_M^{X,VIIa-TF}} \tag{S45}$$

$$D_{Xa-TFPI}\cdot\left.\frac{\partial[Xa-TFPI]}{\partial x}\right|_{\Lambda}=k_a^{VIIa-TF,Xa-TFPI}\cdot[Xa-TFPI]_{\Lambda}\cdot{\sigma_{VIIa-TF}}^{F} \tag{S46}$$

$$D_{TFPI}\cdot\left.\frac{\partial[TFPI]}{\partial x}\right|_{\Lambda}=k_a^{Xa-VIIa-TF,TFPI}\cdot\sigma_{Xa-VIIa-TF}\cdot[TFPI] \tag{S47}$$

It should be noted that for factors that have diffusion terms including free factors (fXa and fIIa), the boundary conditions were written (for Xa^F and IIa^F) as in eq. S44.

1.3. Model parameters

Table S1. Model parameters: initial conditions

1. Initial concentrations for model variables					
Factor	Surface density, 10^6 nmol/mm^2	Factor	Concentration, nM	Factor	Concentration, nM
$\sigma_{VIIa-TF}$	0	VIIa	0.1	VIII	0.7
σ_{VII-TF}	0	VII	10	Va	0
σ_{TF}	special	IXa	0	V	20
		IX	90	APC	0
		Xa	0	PC	60
		X	170	Xa–TFPI	0
		IIa	0	TFPI	2.5
		II	1400	AT-III	3400
		Fn	0	XIa	0
		Fg	7600	XI	30
		VIIIa	0	N_a*	$\delta \cdot 7.5 \cdot 10^{-5}$
2. Constant concentrations in the model					
Factor	Concentration, nM	Factor	Concentration, nM	Factor	Concentration, nM
α_2M	3000	HC-II	1400	PS	346
α_1AT	40000	PCI	88		
α_2AP	1100	C1I	1700		

* N_a, the initial effective procoagulant activity of membranes in plasma, represented by circulating microparticles, lipoproteins, etc., was expressed in activated platelets equivalents (1).

Table S2. Model parameters: kinetic constants.

Constant	Value	Reference
1. Initiation of coagulation		
$k_a^{VIIa,TF}$, $k_d^{VIIa-TF}$	0.0094 $nM^{-1}min^{-1}$, 0.0342 min^{-1}	(4)*
$k_a^{VII,TF}$, k_d^{VII-TF}	0.0094 $nM^{-1}min^{-1}$, 0.0342 min^{-1}	(4)*
$k_{cat}^{VII-TF,IIa}$, $K_M^{VII-TF,IIa}$	3.66 min^{-1}, 2700 nM	(5)
$k_{eff}^{VII-TF,Xa}$	0.4 $nM^{-1}min^{-1}$	(6)
$k_{cat}^{VII,IIa}$, $K_M^{VII,IIa}$	3.66 min^{-1}, 2700 nM	(7)
2. Cascade backbone		
$k_{cat}^{IX,VIIa-TF}$, $K_M^{IX,VIIa-TF}$	6.8 min^{-1}, 250 nM	(8)
$k_d^{Xa-VIIa-TF}$	385 min^{-1}	(9)
$k_{cat}^{IX,XIa}$, $K_M^{IX,XIa}$	5.8 min^{-1}, 200 nM	(10)
$k_{cat}^{X,VIIa-TF}$, $K_M^{X,VIIa-TF}$	20 min^{-1}, 390 nM	(11-13)
$k_{cat}^{X,IXa\,local}$, $K_M^{X,IXa\,local}/k$	0.06 min^{-1}, 230/δ molecules/platelet	(14,15)*,#
$k_{cat}^{X,IXa-VIIIa\,local}$, $K_M^{X,IXa-VIIIa\,local}/k$, $K_d^{IXa-VIIIa\,local}/k$, $K_d^{VIIIa-X\,local}/k$	6350 min^{-1}, 1216/δ molecules/platelet, 278/δ molecules/platelet, 1655/δ molecules/platelet	(16)#
$k_{eff}^{II,Xa}$	45/δ $nM^{-2}min^{-1}$	(17,18)*,#
$\frac{k_{cat}^{local\,II,Xa-Va}}{K_M^{local\,II,Xa-Va}/k}$	0.047·δ min^{-1}	(19)*,#
$k_{cat}^{Fg,IIa}$, $K_M^{Fg,IIa}$	5040 min^{-1}, 7200 nM	(20)
3. Cofactor activation		
$k_{cat}^{VIII,IIa}$, $K_M^{VIII,IIa}$	54 min^{-1}, 147 nM	(21)
$k_{cat}^{V,IIa}$, $K_M^{V,IIa}$	14 min^{-1}, 71.7 nM	(22)
4. Inhibition		
$k_a^{VIIa-TF,Xa-TFPI}$	0.44 $nM^{-1}min^{-1}$	(23)

$k_a^{Xa-VIIa-TF,TFPI}$	6 $nM^{-1}min^{-1}$	(24)
$k_a^{Xa,TFPI}$, $k_d^{Xa-TFPI}$	0.052 $nM^{-1}min^{-1}$, 0.02 min^{-1}	(25)
$k_a^{IXa,AT-III}$	0.0000082 $nM^{-1}min^{-1}$	(26)
$k_a^{Xa,AT-III}$	0.00015 $nM^{-1}min^{-1}$	(27)
k_a^{Xa,α_2M}	0.00004 $nM^{-1}min^{-1}$	(28)
k_a^{Xa,α_1AT}	0.0000136 $nM^{-1}min^{-1}$	(29)
$k_a^{Xa,PCI}$	0.0012 $nM^{-1}min^{-1}$	(30)
$k_a^{Xa-Va^B,AT-III}$	0.000022 $nM^{-1}min^{-1}$	(31)
$k_a^{IIa,AT-III}$	0.00041 $nM^{-1}min^{-1}$	(32)
k_a^{IIa,α_2M}	0.0001 $nM^{-1}min^{-1}$	(33)
k_a^{IIa,α_1AT}	0.000003 $nM^{-1}min^{-1}$	(34)
$k_a^{IIa,PCI}$	0.00037 $nM^{-1}min^{-1}$	(35)
$k_a^{IIa,HC-II}$	0.000063 $nM^{-1}min^{-1}$	(36)
$k_a^{XIa,AT-III}$	0.000019 $nM^{-1}min^{-1}$	(37)
k_a^{XIa,α_2AP}	0.000026 $nM^{-1}min^{-1}$	(38)
k_a^{XIa,α_1AT}	0.000006 $nM^{-1}min^{-1}$	(39)
$k_a^{XIa,PCI}$	0.0054 $nM^{-1}min^{-1}$	(40)
$k_a^{XIa,C1I}$	0.00014 $nM^{-1}min^{-1}$	(41)
k_a^{APC,α_2M}	0.000006 $nM^{-1}min^{-1}$	(42)
k_a^{APC,α_2AP}	0.000006 $nM^{-1}min^{-1}$	(43)
k_a^{APC,α_1AT}	0.0000007 $nM^{-1}min^{-1}$	(44)
$k_a^{APC,PCI}$	0.00039 $nM^{-1}min^{-1}$	(45)
h^{VIIIa}	0.35 min^{-1}	(46)
$k_{eff}^{localVa,APC}$	7.7 $nM^{-1}min^{-1}$	(47)*
$k_{eff}^{PC,APC}$	0.000282 $nM^{-1}min^{-1}$	(48)

$K_i^{Va,PS}$	200 nM	(49)*
$K_i^{VIIIa,PS}$	150 nM	(50)
$k_{cat}^{PC,IIa}$, $K_M^{PC,IIa}$	1.2 min^{-1}, 60000 nM	(51)
5. Long-range feedback		
$k_{eff}^{XI,IIa}$	$0.03/\delta$ $nM^{-2}min^{-1}$	(52)*,#
6. Platelet activation		
$k_{cat}^{N,IIa}$, $K_M^{N,IIa}$	5.4 min^{-1}, 2.4 nM	(53)
$n^{X(II)}$, K_d^X, K_d^{II}	16000/δ sites/platelet, 320 nM, 470 nM	(54)#
n^{VIIIa}, K_d^{VIIIa}	750/δ sites/platelet, 1.5 nM	(55)#
n^{IXa}, K_d^{IXa}	260/δ sites/platelet, 2.57 nM	(56)#
K_d^{Xa-Va}	0.118 nM	(57)
n^{Va}, K_d^{Va}	2700/δ sites/platelet, 2.9 nM	(58,59)#
$\tilde{n}^{Va}$, $\tilde{K}_d^{Va}$	837 sites/platelet, 0.4 nM	(60)
$\rho^{V(a)}$	1000 molecules/platelet	(61)*
δ	0.04	(62,63)

* Estimated on the basis of experimental data.

The values were corrected by a factor of δ or $1/\delta$, compared with the originally reported values that assumed only δ=4% of thrombin-activated platelets actually expose procoagulant membranes and bind coagulation factors (64,65).

§ In the presence of CTI.

Table S3. Model parameters: diffusion coefficients

Model variable	M_r	Diffusion coefficient*, mm^2/min
VIIa	50,000	0.0035
VII.	50,000	0.0035
IXa	46,000	0.0037
IX	57,000	0.0033
Xa	45,000	0.0037
X	58,500	0.0033
IIa	37,000	0.0040
II	72,000	0.0030
Fn	—	0 [#]
Fg	340,000	0.0012 [§]
VIIIa	160,000	0.0021
VIII (+ vWF)	240,000 (+ 500,000-20,000,000)	0 [¶]
Va	150,000	0.0022
V	330,000	0.0016
APC	62,000	0.0032
PC	62,000	0.0032
Xa–TFPI	95,000	0.0027
TFPI	40,000	0.0039
AT-III	58,000	0.0033
XIa	160,000	0.0021
XI.	160,000	0.0021
N_a	$\sim 10^{13}$	0 [‖]

* The values of diffusion coefficients were estimated based on the molecular weights of the components, using data from (66).

[#] Fibrin quickly polymerizes into a fibrin net and was, therefore, assumed not to diffuse.

[§] The value is from (66). Fibrinogen has non-globular shape, and therefore, its estimation on the basis of molecular weight is incorrect.

[¶] FVIII circulates in blood bound to the von Willebrand factor, which forms enormous complexes. We assumed that these complexes do not diffuse.

[‖] Platelets were assumed not to diffuse.

1.4. Model design

The mathematical model for clotting was used to investigate mechanisms of clotting activation by surfaces with different TF distributions. The model mimicked the *in vitro* clotting experiments. Thus, we used 3D calculations in a parallelepiped region with a length of 2 mm and a rectangular base. On this basis, TF was distributed, either uniformly or as rectangular spots at the four corners (imitating ¼ of the fibroblast size). Given the non-permeable boundary conditions, this distribution can be perceived as a continuous field of equidistant TF spots. The size of the base was varied from 0.05×0.09 to 1×1 mm to generate the necessary average TF density at the base (Fig. S1A).

For uniformly distributed TFs, each point on the activation surface had the same TF density. This density was varied by two orders of magnitude from 3 to 100 pmol/m^2.

Fibroblast cells were modeled as rectangular spots. The size of a spot was 60×15 μm. The TF density at the spot was uniform, constant and 500 pmol/m^2. The TF density on the surface between the spots was zero. The average TF density on the surface was varied from 0.5 to 100 pmol/m^2 by varying the distance between adjacent spots from 0.05 to 1 mm.

The spot characteristics were chosen from experimental data, cell monolayer microscopy and TF activity assays. Fibroblasts on the film were "spread-eagle" spindle-shaped cells (Fig. S4), with a length of 71±12 μm and a maximum width of 11±3 μm (n=14). The average cell area was 800±150 μm ^{2}. The average TF density was measured by testing TF activity over the same series of films. TF activity was 135±13 pmol/m^2 for an average cell density of 290±30 cells/mm^2. Thus, the TF density at the fibroblasts was 580±140 pmol/m^2.

Clot growth parameters were calculated as average parameters across the surface to better correspond with the spatial experiments. The average fibrin concentration was calculated as a mean concentration at some distance from the surface and treated as the light scattering profiles from the experiments (see Materials and Methods). We assumed that the fibrin concentration was proportional to the optical properties of the clot (67). The principal mechanism for this calculation is shown in Fig. S1.

To evaluate any effect of differences in K_d between the cells and immobilized TF (68) on the phenomena observed herein, we performed additional computer simulations in which we altered this parameter 3-fold in several directions (either increasing association rate or decreasing dissociation rate). The K_d did not affect the difference between uniformly immobilized TF and TF spots (Fig. S2).

1.5. Roles of factors V and VII activation feedback loops in sensitivity to local TF density

The calculation of clot growth parameters in a normal model and in a model without fV and fVII activation is shown in Fig. S3. The data herein demonstrates that the positive feedback loops for fV activation by thrombin and fVII activation by fXa are necessary to sense local TF surface density. Without these feedback loops, the initiation time was independent of surface TF distribution. The addition of these feedback loops to the system yielded a difference in initiation times.

2. Experiments

2.1. Expanded Methods

Preparation of the fibroblast films. The fibroblast suspensions were prepared in RPMI medium (Sigma, St Louis, MO, USA) with HEPES buffer at concentrations ranging from 2×10^3 to 96×10^3 cells/ml. They were placed on a 24-well plate (Nunc, Rochester, NY, USA) with polyethylene terephthalate films (Joint Institute for Nuclear Research, Dubna, Russia). Cell density was routinely measured for a typical film from each series before the clot growth experiments. The cell-containing films were dyed with acridine orange and imaged with the fluorescent microscope Leica DM/RBE (Leica, Wetzlar, Germany), and the cell density was calculated (Fig. S4, S8). The densities decreased following the decrease in suspended cell concentration. The maximum density for cell monolayers was approximately 1000 cells/mm^2, and its variation (SD) did not exceed 10% among either the different films for each series or different portions of each film. For the minimal suspended cell concentration (2×10^3 cells/ml), the film surface was covered with detached and sparsely located fibroblasts, and the fibroblast density was approximately 11±6 cells/mm^2 (confidence level 0.9). The average density of functional TF on the films was measured using the Actichrome-TF kit (American Diagnostica, Stamford, CT, USA).

TF immobilization on the films. Thromboplastin (Renam, Moscow, Russia) was dissolved in deionized water and dialyzed three times at +4^{o}C for 24 h against 0.05 M PBS, pH 7.2 – 7.4 (Sigma), containing 0.1% Triton X–100 (Sigma, USA). Subsequently, the solution was centrifuged at 10,000 g for 5 min, and the supernatant protein concentration was measured using the Lowry method. Ten microliters of sulfosuccinimidyl-6-(biotinamido) hexanoate (EZ-Link^{TM} Sulfo-NHS-LC-Biotin, Pierce, Rockford, IL, USA) at a concentration of 17.7 mg/ml was added to 0.5 ml thromboplastin solution in PBS with 0.1% Triton X–100 (protein concentration was 3.1 mg/ml). The reaction proceeded for 3 h at room temperature with continuous shaking. Afterward, biotinylated thromboplastin was dialyzed at

+4°C for 24 h against PBS containing 0.1% Triton X–100. Films with streptavidin were incubated with biotinylated thromboplastin solutions at different concentrations for 30 min at room temperature with continuous shaking. The prepared films were stored at -20 C in 50% glycerol over 6 months with constant TF activity. The average density of functional TF on the films was measured using the Actichrome-TF kit (American Diagnostica, Stamford, CT, USA).

Assembly of intrinsic tenase on films with immobilized TF or fibroblasts. The ability of the TF-bearing films to provide binding sites for intrinsic tenase was evaluated based on their acceleration of fX activation. The 2×2 mm^2 films contained either immobilized TF or with fibroblasts with a mean TF surface density of 120 pmol/m^2 and were incubated in 20 μl of buffer A (150 mM NaCl, 2.7 mM KCl, 1 mM $MgCl_2$, 0.4 mM NaH_2PO_4, 20 mM HEPES, 5 mM glucose, 0.5% bovine serum albumin) with 5 mM $CaCl_2$. To evaluate intrinsic tenase assembly, the samples were supplemented with 20 μl of a mixture containing 0.2 nM fIXa, 40 nM fVIIIa, and 800 nM fX. FVIIIa was prepared immediately prior to the experiment by incubation with 40 nM fVIII and 1 nM thrombin for 1 min, followed by 2 μM PPACK addition. After 4 min at 37°C with shaking, fX activation was stopped using EDTA (40 μl at 20 mM), and fXa activity was evaluated by the rate of S2765 hydrolysis that was measured using absorbance at 405 nm in a Thermomax microplate reader (Molecular Devices, Sunnyvale, CA).

Assembly of prothrombinase on films with either immobilized TF or fibroblasts. To evaluate prothrombinase-supporting activity, the 2×2 mm^2 films were incubated with 20 μl buffer A containing 3.75 mM $CaCl_2$ and supplemented with 10 μl of a mixture containing 30 nM fXa, 6 nM RVV-V activated fV, and 4200 nM prothrombin. After 5 min at 37°C with shaking, the reaction was stopped using EDTA (270 μl at 5.6 mM). Thrombin activity was evaluated by the rate of Gly-Pro-Arg-NA hydrolysis measured using a Thermomax reader.

Spatial clot growth in the reaction-diffusion system and image processing. The experimental chamber was assembled in a 35-mm polystyrene Petri dish (Biomedical Ltd, Moscow, Russia) with a 1 mm-thick microscope glass slide (VWR Scientific Inc., West Chester, PA, USA) fixed to the bottom. The glass slide edge, which formed a vertical wall of the chamber, was wrapped in either cell-coated film or film with immobilized TF and covered with a piece of black polystyrene that formed the upper surface of the chamber. Recalcified plasma was transferred into the assembled chamber, and the dish was sealed and placed in a temperature-controlled water jacket at 37ºC. The microchamber was illuminated from below with red light-emitting diodes L-1543-E at a peak wavelength 660 nm (Kingbright, Tokyo, Japan) and 135° to the direction of recording. The light scattering image was recorded every 30 sec using a SFW-1310M camera (Scion Corporation, Frederick, MD, USA) and processed as described below.

The images (Fig. 2A) were used to generate plots of light scattering intensity versus distance from the TF-bearing surface at different time points (Fig. 2B) and clot size versus time (Fig. 2C). The *initiation time* for clot formation was defined as the time interval required for mean light scattering intensity near the activator to reach the half-maximum value for a clot activated by the film at maximum TF density. For each frame, clot size was determined as the distance between the activation film and the clot edge (clot edge was defined as the point where the light scattering intensity was equal to the half-maximum value for a clot activated by the film at maximum TF density). The *rate of clot growth* was derived from the clot size versus time curve as a mean rate ranging from 10 to 40 min following the onset of clotting. The *clot size after 40 min* from the clotting activation was also recorded. These measurements were performed for three different areas in the image for each set of experimental images.

2.2. Stability of the studied plasma

To test whether incubation of the thawed plasma affects clotting parameters, we performed control experiments and showed that both the APTT and spatial clot formation parameters in normal plasma were unchanged for 48 h (Fig. S5).

2.3. Images of fibrin clots for different densities of immobilized TF and TF-bearing cells

Figs. S6 and S7 demonstrate clot formation from at surfaces with uniform TF distribution and fibroblast monolayers, respectively. TF density was varied from 1.4 to 135 pmol/m^2. To characterize the cell monolayers, the average distance between cells was calculated using pictures of the cell monolayers. This distance varied from 300 to 50 μm (see Fig. S8). Clotting was equally rapid for the films with different cell densities (see Fig. S7). Considering the small diffusion coefficients for clotting enzymes (Table S3) and characteristic times for the initial phase of clotting (within 10 min), we conclude that a single cell is sufficient to initiate clotting.

2.4. Images of fibrin clots for fV-, fVII- and fVIII-deficient plasma

Fig. S9 demonstrates clotting in fV-, fVII and fVIII-deficient plasma. The data are shown for two types of activation, uniformly distributed TF and fibroblast-containing films. In fV- and fVII-deficient plasma, the difference in clot growth activated by surfaces with different TF distributions was minimal, whereas the difference in fVIII-deficient plasma was similar to normal plasma. Further, in plasma

without fV and fVIII, the clot profiles were diffusive. Thus, the resulting fibrin clot did not have a sharp boundary between the solid clot and liquid plasma.

2.5. Comparison of clot growth parameters in the deficient plasma

Fig. S10 shows the clot growth parameters obtained from the mathematical model and experiments, which demonstrate the role of fV and fVII activation in endowing pattern recognition on the clotting system. In the normal and fVIII-deficient plasma, clotting was slow for low TF density activation but rapid for activation with cells at the same average TF density. In contrast, the clot growth parameters were the same as for fV- and fVII-deficient plasma. The theoretical and experimental data correlated well. Absent fVIII, the clot growth rate was two-fold smaller than in normal plasma.

2.6. Explanation of the role of positive feedback from fV activation in clotting

Fibrin clots in plasma without fV and fVIII had more diffuse profiles than normal plasma and plasma without fVII (Fig. S11). This result might be explained by the lack of the critically important positive feedback loops required for creating explosive thrombin production. Such loose clots might provide an explanation for the thromboembolic tendencies reported in certain fV-deficient patients (69,70).

References

1. Panteleev, M. A., M. V. Ovanesov, D. A. Kireev, A. M. Shibeko, E. I. Sinauridze, N. M. Ananyeva, A. A. Butylin, E. L. Saenko, and F. I. Ataullakhanov. 2006. Spatial propagation and localization of blood coagulation are regulated by intrinsic and protein C pathways, respectively. *Biophys. J.* 90:1489-1500.
2. Sinauridze, E. I., D. A. Kireev, N. Y. Popenko, A. V. Pichugin, M. A. Panteleev, O. V. Krymskaya, and F. I. Ataullakhanov. 2007. Platelet microparticle membranes have 50- to 100-fold higher specific procoagulant activity than activated platelets. *Thromb. Haemost.* 97:425-434.
3. Panteleev, M. A., E. L. Saenko, N. M. Ananyeva, and F. I. Ataullakhanov. 2004. Kinetics of factor X activation by the membrane-bound complex of factor IXa and factor VIIIa. *Biochem. J.* 381:779-794.
4. Petersen LC, Olsen OH, Nielsen LS, Freskgard PO and Persson E. 2000. Binding of Zn2+ to a Ca2+ loop allosterically attenuates the activity of factor VIIa and reduces its affinity for tissue factor. *Protein Sci* 9:859-866.
5. Butenas, S. and K. G. Mann. 1996. Kinetics of human factor VII activation. *Biochemistry* 35:1904-1910.
6. Rao, L. V., T. Williams, and S. I. Rapaport. 1996. Studies of the activation of factor VII bound to tissue factor. *Blood* 87:3738-3748.
7. Butenas, S. and K. G. Mann. 1996. Kinetics of human factor VII activation. *Biochemistry* 35:1904-1910.
8. Komiyama, Y., A. H. Pedersen, and W. Kisiel. 1990. Proteolytic activation of human factors IX and X by recombinant human factor VIIa: effects of calcium, phospholipids, and tissue factor. *Biochemistry* 29:9418-9425.
9. Panteleev MA, Zarnitsina VI, and Ataullakhanov FI. 2002. Tissue factor pathway inhibitor: a possible mechanism of action. *Eur J Biochem* 269:2016-2031.
10. Gailani, D., D. Ho, M. F. Sun, Q. Cheng, and P. N. Walsh. 2001. Model for a factor IX activation complex on blood platelets: dimeric conformation of factor XIa is essential. *Blood* 97:3117-3122.
11. Baugh, R. J. and S. Krishnaswamy. 1996. Role of the activation peptide domain in human factor X activation by the extrinsic Xase complex. *J. Biol. Chem.* 271:16126-16134.
12. Komiyama, Y., A. H. Pedersen, and W. Kisiel. 1990. Proteolytic activation of human factors IX and X by recombinant human factor VIIa: effects of calcium, phospholipids, and tissue factor. *Biochemistry* 29:9418-9425.
13. Krishnaswamy S, Field KA, Edgington TS, Morrissey JH, and Mann KG. 1992. Role of the membrane surface in the activation of human coagulation factor X. *J Biol Chem* 267:26110-26120.
14. Scandura, J. M. and P. N. Walsh. 1996. Factor X bound to the surface of activated human platelets is preferentially activated by platelet-bound factor IXa. *Biochemistry* 35:8903-8913.
15. Rawala-Sheikh, R., S. S. Ahmad, B. Ashby, and P. N. Walsh. 1990. Kinetics of coagulation factor X activation by platelet-bound factor IXa. *Biochemistry* 29:2606-2611.
16. Panteleev, M. A., E. L. Saenko, N. M. Ananyeva, and F. I. Ataullakhanov. 2004. Kinetics of factor X activation by the membrane-bound complex of factor IXa and factor VIIIa. *Biochem. J.* 381:779-794.
17. Tracy, P. B., L. L. Eide, and K. G. Mann. 1985. Human prothrombinase complex assembly and function on isolated peripheral blood cell populations. *J. Biol. Chem.* 260:2119-2124.
18. van Dieijen, G., G. Tans, J. Rosing, and H. C. Hemker. 1981. The role of phospholipid and factor VIIIa in the activation of bovine factor X. *J. Biol. Chem.* 256:3433-3442.

19. Tracy, P. B., L. L. Eide, and K. G. Mann. 1985. Human prothrombinase complex assembly and function on isolated peripheral blood cell populations. *J. Biol. Chem.* 260:2119-2124.
20. Higgins, D. L., S. D. Lewis, and J. A. Shafer. 1983. Steady state kinetic parameters for the thrombin-catalyzed conversion of human fibrinogen to fibrin. *J. Biol. Chem.* 258:9276-9282.
21. Hill-Eubanks, D. C. and P. Lollar. 1990. von Willebrand factor is a cofactor for thrombin-catalyzed cleavage of the factor VIII light chain. *J. Biol. Chem.* 265:17854-17858.
22. Monkovic, D. D. and P. B. Tracy. 1990. Activation of human factor V by factor Xa and thrombin. *Biochemistry* 29:1118-1128.
23. Baugh, R. J., G. J. Broze, Jr., and S. Krishnaswamy. 1998. Regulation of extrinsic pathway factor Xa formation by tissue factor pathway inhibitor. *J. Biol. Chem.* 273:4378-4386.
24. Panteleev, M. A., V. I. Zarnitsina, and F. I. Ataullakhanov. 2002. Tissue factor pathway inhibitor: a possible mechanism of action. *Eur. J. Biochem.* 269:2016-2031.
25. Baugh, R. J., G. J. Broze, Jr., and S. Krishnaswamy. 1998. Regulation of extrinsic pathway factor Xa formation by tissue factor pathway inhibitor. *J. Biol. Chem.* 273:4378-4386.
26. Pieters, J., G. Willems, H. C. Hemker, and T. Lindhout. 1988. Inhibition of factor IXa and factor Xa by antithrombin III/heparin during factor X activation. *J. Biol. Chem.* 263:15313-15318.
27. Rezaie, A. R. 1998. Calcium enhances heparin catalysis of the antithrombin-factor Xa reaction by a template mechanism. Evidence that calcium alleviates Gla domain antagonism of heparin binding to factor Xa. *J. Biol. Chem.* 273:16824-16827.
28. Ellis, V., M. Scully, I. MacGregor, and V. Kakkar. 1982. Inhibition of human factor Xa by various plasma protease inhibitors. *Biochim. Biophys. Acta* 701:24-31.
29. Ellis, V., M. Scully, I. MacGregor, and V. Kakkar. 1982. Inhibition of human factor Xa by various plasma protease inhibitors. *Biochim. Biophys. Acta* 701:24-31.
30. Espana, F., M. Berrettini, and J. H. Griffin. 1989. Purification and characterization of plasma protein C inhibitor. *Thromb. Res.* 55:369-384.
31. Ellis, V., M. F. Scully, and V. V. Kakkar. 1984. Inhibition of prothrombinase complex by plasma proteinase inhibitors. *Biochemistry* 23:5882-5887.
32. Rezaie, A. R. 1998. Calcium enhances heparin catalysis of the antithrombin-factor Xa reaction by a template mechanism. Evidence that calcium alleviates Gla domain antagonism of heparin binding to factor Xa. *J. Biol. Chem.* 273:16824-16827.
33. Jesty, J. 1986. The kinetics of inhibition of alpha-thrombin in human plasma. *J. Biol. Chem.* 261:10313-10318.
34. Heeb, M. J., R. Bischoff, M. Courtney, and J. H. Griffin. 1990. Inhibition of activated protein C by recombinant alpha 1-antitrypsin variants with substitution of arginine or leucine for methionine358. *J. Biol. Chem.* 265:2365-2369.
35. Espana, F., M. Berrettini, and J. H. Griffin. 1989. Purification and characterization of plasma protein C inhibitor. *Thromb. Res.* 55:369-384.
36. Derechin, V. M., M. A. Blinder, and D. M. Tollefsen. 1990. Substitution of arginine for Leu444 in the reactive site of heparin cofactor II enhances the rate of thrombin inhibition. *J. Biol. Chem.* 265:5623-5628.
37. Wuillemin, W. A., E. Eldering, F. Citarella, C. P. de Ruig, H. ten Cate, and C. E. Hack. 1996. Modulation of contact system proteases by glycosaminoglycans. Selective enhancement of the inhibition of factor XIa. *J. Biol. Chem.* 271:12913-12918.
38. Wuillemin, W. A., E. Eldering, F. Citarella, C. P. de Ruig, H. ten Cate, and C. E. Hack. 1996. Modulation of contact system proteases by glycosaminoglycans. Selective enhancement of the inhibition of factor XIa. *J. Biol. Chem.* 271:12913-12918.
39. Wuillemin, W. A., E. Eldering, F. Citarella, C. P. de Ruig, H. ten Cate, and C. E. Hack. 1996. Modulation of contact system proteases by glycosaminoglycans. Selective enhancement of the inhibition of factor XIa. *J. Biol. Chem.* 271:12913-12918.

40. Espana, F., M. Berrettini, and J. H. Griffin. 1989. Purification and characterization of plasma protein C inhibitor. *Thromb. Res.* 55:369-384.
41. Meijers, J. C., R. A. Vlooswijk, and B. N. Bouma. 1988. Inhibition of human blood coagulation factor XIa by C-1 inhibitor. *Biochemistry* 27:959-963.
42. Heeb, M. J., A. Gruber, and J. H. Griffin. 1991. Identification of divalent metal ion-dependent inhibition of activated protein C by alpha 2-macroglobulin and alpha 2-antiplasmin in blood and comparisons to inhibition of factor Xa, thrombin, and plasmin. *J. Biol. Chem.* 266:17606-17612.
43. Heeb, M. J., A. Gruber, and J. H. Griffin. 1991. Identification of divalent metal ion-dependent inhibition of activated protein C by alpha 2-macroglobulin and alpha 2-antiplasmin in blood and comparisons to inhibition of factor Xa, thrombin, and plasmin. *J. Biol. Chem.* 266:17606-17612.
44. Heeb, M. J., R. Bischoff, M. Courtney, and J. H. Griffin. 1990. Inhibition of activated protein C by recombinant alpha 1-antitrypsin variants with substitution of arginine or leucine for methionine358. *J. Biol. Chem.* 265:2365-2369.
45. Espana, F., M. Berrettini, and J. H. Griffin. 1989. Purification and characterization of plasma protein C inhibitor. *Thromb. Res.* 55:369-384.
46. Lollar, P., E. T. Parker, and P. J. Fay. 1992. Coagulant properties of hybrid human/porcine factor VIII molecules. *J. Biol. Chem.* 267:23652-23657.
47. Solymoss, S., M. M. Tucker, and P. B. Tracy. 1988. Kinetics of inactivation of membrane-bound factor Va by activated protein C. Protein S modulates factor Xa protection. *J. Biol. Chem.* 263:14884-14890.
48. Hassouna, H. and C. Quinn. 2002. Proteolysis of protein C in pooled normal plasma and purified protein C by activated protein C (APC). *Biophys. Chem.* 95:109-124.
49. Hackeng, T. M., '. van, V, J. C. Meijers, and B. N. Bouma. 1994. Human protein S inhibits prothrombinase complex activity on endothelial cells and platelets via direct interactions with factors Va and Xa. *J. Biol. Chem.* 269:21051-21058.
50. Koppelman, S. J., T. M. Hackeng, J. J. Sixma, and B. N. Bouma. 1995. Inhibition of the intrinsic factor X activating complex by protein S: evidence for a specific binding of protein S to factor VIII. *Blood* 86:1062-1071.
51. Esmon, N. L., L. E. DeBault, and C. T. Esmon. 1983. Proteolytic formation and properties of gamma-carboxyglutamic acid-domainless protein C. *J. Biol. Chem.* 258:5548-5553.
52. Oliver, J. A., D. M. Monroe, H. R. Roberts, and M. Hoffman. 1999. Thrombin activates factor XI on activated platelets in the absence of factor XII. *Arterioscler. Thromb. Vasc. Biol.* 19:170-177.
53. Smith, R. D. and W. G. Owen. 1999. Platelet responses to compound interactions with thrombin. *Biochemistry* 38:8936-8947.
54. Scandura, J. M., S. S. Ahmad, and P. N. Walsh. 1996. A binding site expressed on the surface of activated human platelets is shared by factor X and prothrombin. *Biochemistry* 35:8890-8902.
55. Ahmad, S. S., J. M. Scandura, and P. N. Walsh. 2000. Structural and functional characterization of platelet receptor-mediated factor VIII binding. *J. Biol. Chem.* 275:13071-13081.
56. Ahmad, S. S., R. Rawala-Sheikh, and P. N. Walsh. 1989. Comparative interactions of factor IX and factor IXa with human platelets. *J. Biol. Chem.* 264:3244-3251.
57. Tracy, P. B., L. L. Eide, and K. G. Mann. 1985. Human prothrombinase complex assembly and function on isolated peripheral blood cell populations. *J. Biol. Chem.* 260:2119-2124.
58. Tracy, P. B., L. L. Eide, and K. G. Mann. 1985. Human prothrombinase complex assembly and function on isolated peripheral blood cell populations. *J. Biol. Chem.* 260:2119-2124.
59. Tracy, P. B., M. E. Nesheim, and K. G. Mann. 1992. Platelet factor Xa receptor. *Methods Enzymol.* 215:329-360.
60. Tracy, P. B., M. E. Nesheim, and K. G. Mann. 1981. Coordinate binding of factor Va and factor Xa to the unstimulated platelet. *J Biol. Chem.* 256:743-751.

61. Baruch, D., H. C. Hemker, and T. Lindhout. 1986. Kinetics of thrombin-induced release and activation of platelet factor V. *Eur. J. Biochem.* 154:213-218.
62. Panteleev, M. A., N. M. Ananyeva, N. J. Greco, F. I. Ataullakhanov, and E. L. Saenko. 2005. Two subpopulations of thrombin-activated platelets differ in their binding of the components of the intrinsic factor X-activating complex. *J. Thromb. Haemost.* 3:2545-2553.
63. London, F. S., M. Marcinkiewicz, and P. N. Walsh. 2004. A subpopulation of platelets responds to thrombin- or SFLLRN-stimulation with binding sites for factor IXa. *J. Biol. Chem.* 279:19854-19859.
64. Panteleev, M. A., N. M. Ananyeva, N. J. Greco, F. I. Ataullakhanov, and E. L. Saenko. 2005. Two subpopulations of thrombin-activated platelets differ in their binding of the components of the intrinsic factor X-activating complex. *J. Thromb. Haemost.* 3:2545-2553.
65. London, F. S., M. Marcinkiewicz, and P. N. Walsh. 2004. A subpopulation of platelets responds to thrombin- or SFLLRN-stimulation with binding sites for factor IXa. *J. Biol. Chem.* 279:19854-19859.
66. Marshal, A. G. 1978. Biological chemistry: principles, technics, and applications. John Wiley and Sons, New York.
67. Ovanesov, M. V., N. M. Ananyeva, M. A. Panteleev, F. I. Ataullakhanov, and E. L. Saenko. 2005. Initiation and propagation of coagulation from tissue factor-bearing cell monolayers to plasma: initiator cells do not regulate spatial growth rate. *J. Thromb. Haemost.* 3:321-331.
68. Fadeeva, O. A., M. A. Panteleev, S. S. Karamzin, A. N. Balandina, I. V. Smirnov, and F. I. Ataullakhanov. 2010. Thromboplastin immobilized on polystyrene surface exhibits kinetic characteristics close to those for the native protein and activates in vitro blood coagulation similarly to thromboplastin on fibroblasts. *Biochemistry (Mosc.)* 75:734-743.
69. Manotti, C., R. Quintavalla, M. Pini, M. Jeran, M. Paolicelli, and A. G. Dettori. 1989. Thromboembolic manifestations and congenital factor V deficiency: a family study. *Haemostasis* 19:331-334.
70. Reich, N. E., G. C. Hoffman, V. G. deWolfe, and H. S. Van Ordstrand. 1976. Recurrent thrombophlebitis and pulmonary emboli in congenital factor 5 deficiency. *Chest* 69:113-114.

Figure legends

Fig. S1. Design of the in silico experiments. A – Calculation area and TF distribution (pink) for the uniformly distributed TF (top) and activation with the high density TF spots (bottom). The average TF density at the bottom surface was 6.25 pmol/m^2 in both cases. TF density at the spots was 500 pmol/m^2. **B** – Fibrin concentration distribution for uniformly distributed TFs (top) and the high TF density spots (bottom) at different time points after activation was initiated. The colors indicate the fibrin concentration in parallelepipeds. The one-dimensional fibrin distribution along the red arrows (numbers 1 and 2) was calculated in panel **C**. The all-surfaces-averaged (not limited to the panel **C** plots) fibrin distribution and corresponding clot size plots as a function of time are shown on **D**. Red arrows indicate the position initiation time.

Fig. S2. Effect of TF–fVII/VIIa association/dissociation velocities on the difference between uniformly immobilized and spotted TFs.

Fig. S3. Positive feedback loops from fV and fVII activation supplied a difference in fibrin production dynamics at a surface with uniformly distributed and spotted TFs. The average TF density at the bottom surface was 12.5 pmol/m^2 in both cases. The TF density at the spots was 500 pmol/m^2. **A** – Fibrin concentration distribution for the uniformly distributed TFs (top) and for the high TF density spots (bottom) for a normal model (left) and a model without fV activation by thrombin and fVII activation by FXa (right). The data after 40 min from the initiation of activation are shown. The colors indicate the fibrin concentration in parallelepipeds. To enhance clot activation, the plasma without feedback loops was supplemented with fVa (1% of normal fV concentrations). The one-dimensional fibrin distribution along the red arrows (numbers 1 and 2) was calculated in panels **B** and **C**. The all-surfaces-averaged (not limited to the panel B and C plots) fibrin distribution and corresponding clot size plots as a function of time are shown in **D**. The pink area indicates differences in initiation times that depend on TF distribution in the normal model. The red line indicates the corresponding initiation times in the model without feedback loops.

Fig. S4. Images of fibroblast monolayers with different cell densities that were used for clotting activation. Fibroblast densities were 1000 (**A**), 350 (**B**), and 90 (**C**) cells/mm^2. Cells were grown on polyethylene terephthalate films placed at the bottom of plate wells filled with a cell suspension at

different concentrations. The cells were dyed with acridine orange and imaged using a fluorescent microscope.

Fig. S5. Dependence of APTT (A) on clotting initiation time (B) and spatial clot formation velocity (C) in normal plasma upon storage. Spatial clotting was activated by immobilized TFs at a surface density of 85 pmol/m^2. The mean values ± S.D. are shown.

Fig. S6. The effect of uniformly immobilized TFs on fibrin clot growth in normal plasma strongly depends on TF density. Typical experimental results for platelet-free plasma coagulation activated with TF at 96, 21 and 6 pmol/m^2 are shown. **A.** Images of fibrin clots at different TF densities. During the experiment (2 h), large fibrin clots were formed on the films with high TF densities, but no clot formation was detected for clotting activation at the lowest TF density. Where TF density was lowest, the clot formation was delayed, and the size was smaller. **B.** Corresponding profiles for clot growth. **C.** Clot size as a function of time. Each curve (profile) corresponds to a different time point during clot growth, and the left and lowest curve corresponds to 5 min after recalcification; the subsequent curves are separated by 5-min intervals. As the size of the clot increased, the curves shift upward (implying that the clot is denser) and to the right (the clot becomes larger). The first 50 minutes are shown. **C.** Clot size as a function of time. The plots were obtained using the series of profiles shown in panel B.

Fig. S7. Clot formation is insensitive to fibroblast density. Typical experimental results for platelet-free plasma coagulation activated by fibroblast monolayers with average TF densities of 120, 56 and 3.4 pmol/m^2 are shown. **A.** Images of fibrin clots from different TF densities as recorded by light scattering are shown. Clotting was performed in thin layers of plasma from healthy donors. The activating surface was located on the vertical wall of the experimental chamber and is shown as a vertical stripe at the left end of each image. **B.** Corresponding profiles of clot growth. **C.** Clot size as a function of time. All conditions are as in Fig. S4

Fig. S8. Fibroblast monolayer characterization. The average distance between adjacent cells depended on the average TF density on the film, as shown. (n=3, error bars are SD).

Fig. S9. Feedback loops for fV and fVIII activation form a clear boundary between fibrin clot and liquid plasma. A. Typical experimental results for clotting activation by immobilized TFs or fibroblasts surface with an average TF density of 8 pmol/m^2 are shown. **A.** Images of fibrin clots at

different TF densities. Clotting was performed in thin layers of fV-, fVII- and fVIII-deficient patient plasma. To enhance clot activation, fV-deficient plasma (<1%) was supplemented with Va (0.1% of the normal fV concentration) and fVII-deficient plasma (<1%) was supplemented with VIIa (1% of the normal fVII concentration). Clot growth in fV- and fVII-deficient plasma was independent of activator type, whereas in fVIII-deficient plasma, clots grew only from the fibroblast layer. **B.** Corresponding profiles of clot growth. Clot profiles were diffuse for fV- and fVIII-deficient plasma, whereas in fVII-deficient plasma, a clear boundary between the fibrin clot and liquid plasma was formed. **C.** Clot size as a function of time. All conditions are as in Fig. S4.

Fig. S10. Roles of the positive feedback loops for fV and fVII activation in clot formation during activation by either fibroblasts or immobilized TFs. To test the mathematical model prediction that the clotting system can recognize activator patterns with through fV and fVII activation only, we performed experiments with fV-, fVII and fVIII-deficient plasma. The mathematical model (left panel) and experimental data (right panel) are shown. The average TF density is 6.25 pmol/m^2 for the mathematical model and 8 pmol/m^2 for the experiments. Plots show initiation time (**A**), clot growth rate (**B**), and clot size at t=40 min (**C**) for the control plasma and fV-, fVII-, and fVIII-deficient plasma. Immobilized TF and TF-bearing cells were used for clotting activation. As a control, a mixture of fV- and fVII-deficient plasma at a 1/1 volume ratio was used. To enhance clotting activation, fV-deficient plasma (<1%) was supplemented with fVa (0.1% of the normal fV concentration) and fVII-deficient plasma (<1%) was supplemented with VIIa (1% of the normal fVII concentration). Control and fVIII-deficient plasma were sensitive to TF distribution, whereas fV- and fVII-deficient plasma had only slight activation differences with uniformly immobilized TF or with fibroblasts.

Fig. S11. Clot profile differences in fV-, fVII-, and fVIII-deficient plasma. Clot profiles at 50 min after experiment initiation are shown. Clotting was activated by either immobilized TF (**A**) or a fibroblast monolayer (**B**). The average TF density was the same in these two cases and equaled 8 pmol/m^2. In fV- and fVIII-deficient plasma, clot profiles had a more diffuse shape than in the fVII-deficient plasma.

Figures

Fig. S1

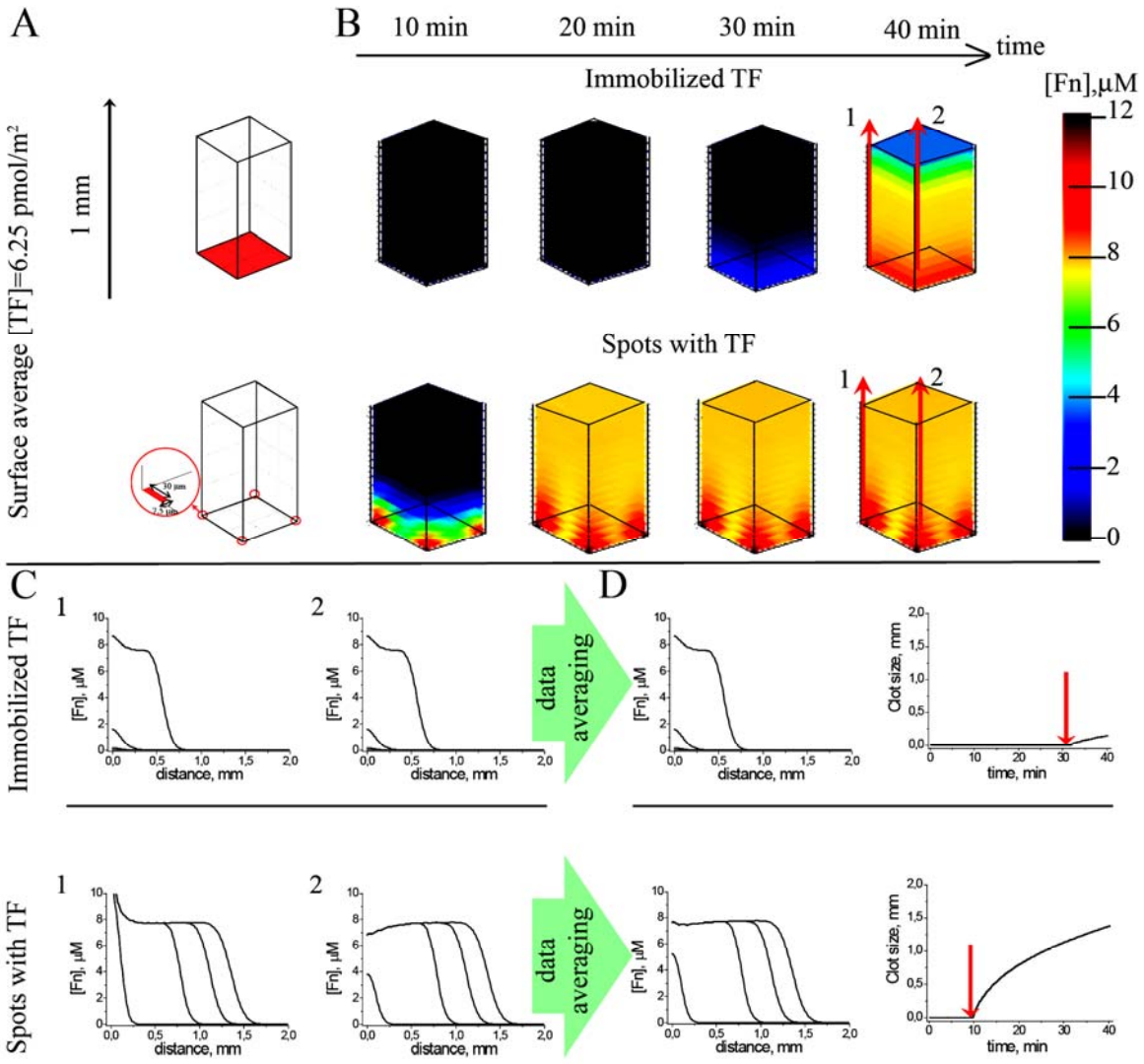

Fig. S2

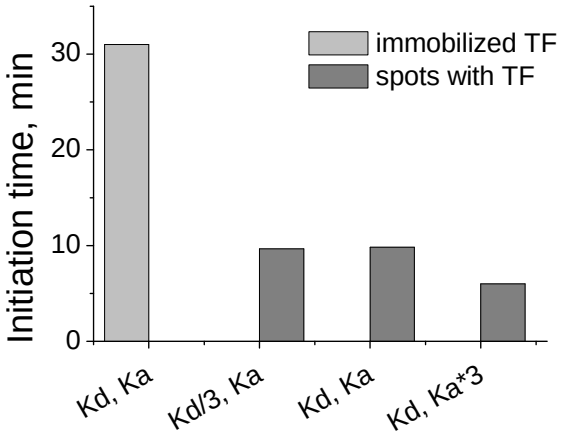
immobilized TF
spots with TF
Initiation time, min
0
10
20
30
Kd, Ka
Kd/3, Ka
Kd, Ka
Kd, Ka*3

Fig. S3

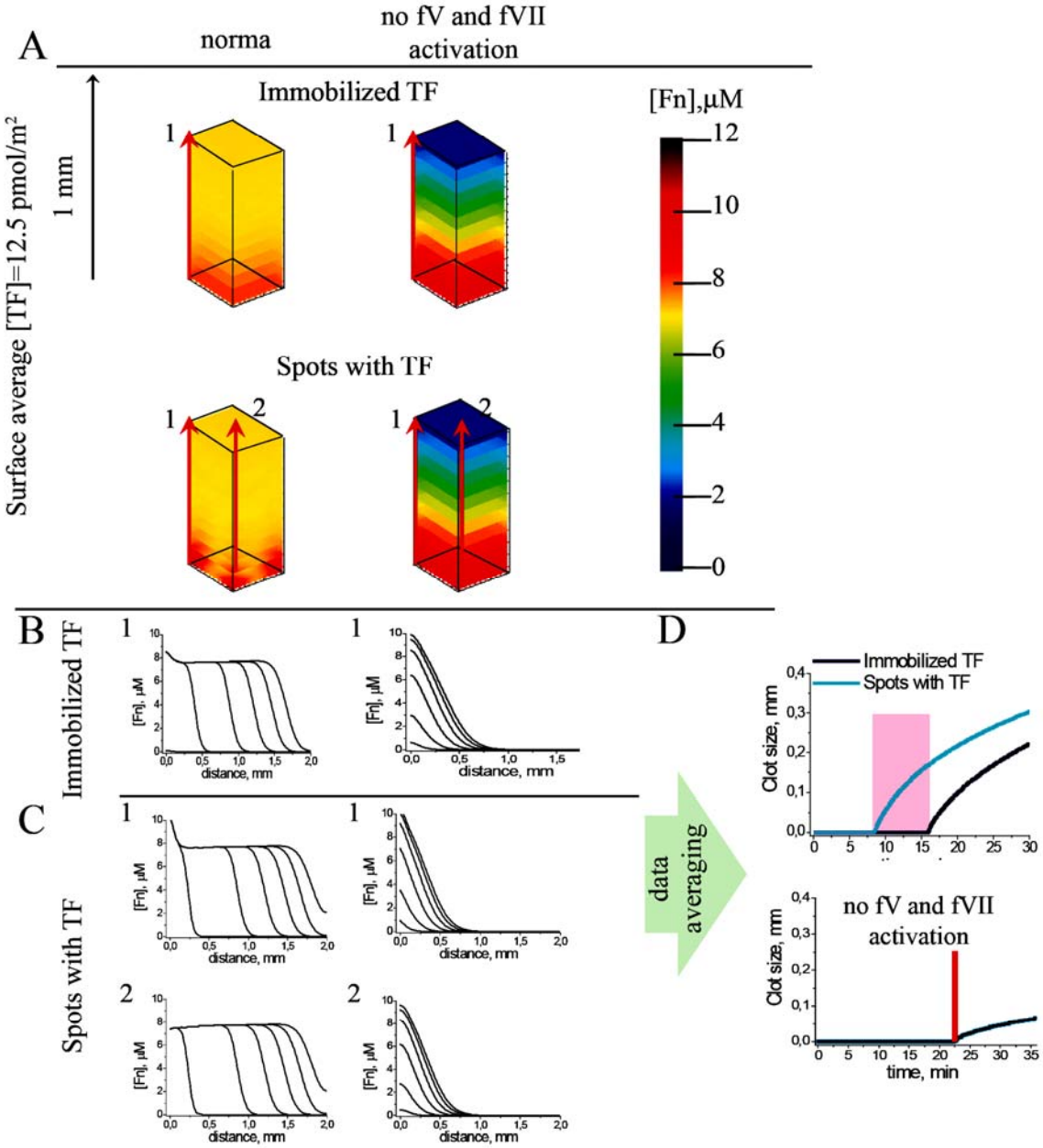
A
norma
no fV and fVII activation
Immobilized TF
Spots with TF
Surface average [TF]=12.5 pmol/m²
1 mm
[Fn],μM
12
10
8
6
4
2
0
B
Immobilized TF
C
Spots with TF
[Fn], μM
distance, mm
D
data averaging
Immobilized TF
Spots with TF
Clot size, mm
no fV and fVII activation
time, min

Fig. S4

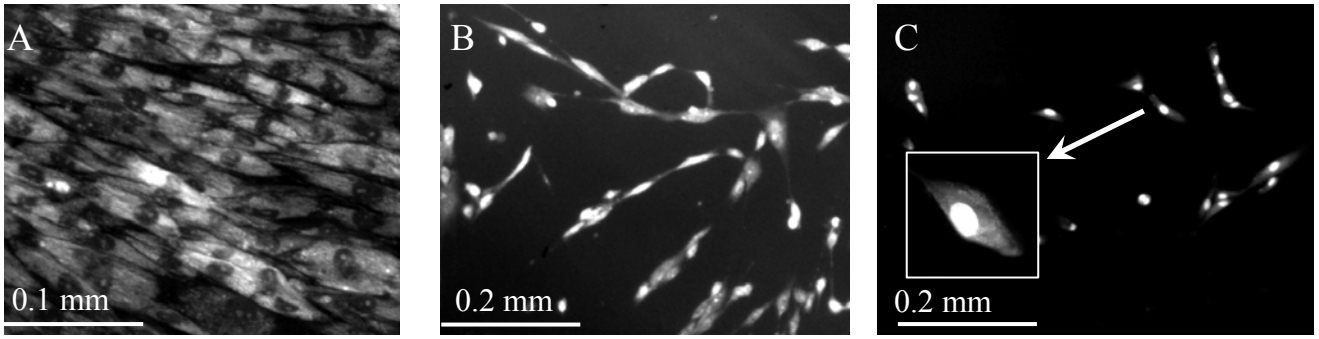

Fig. S5

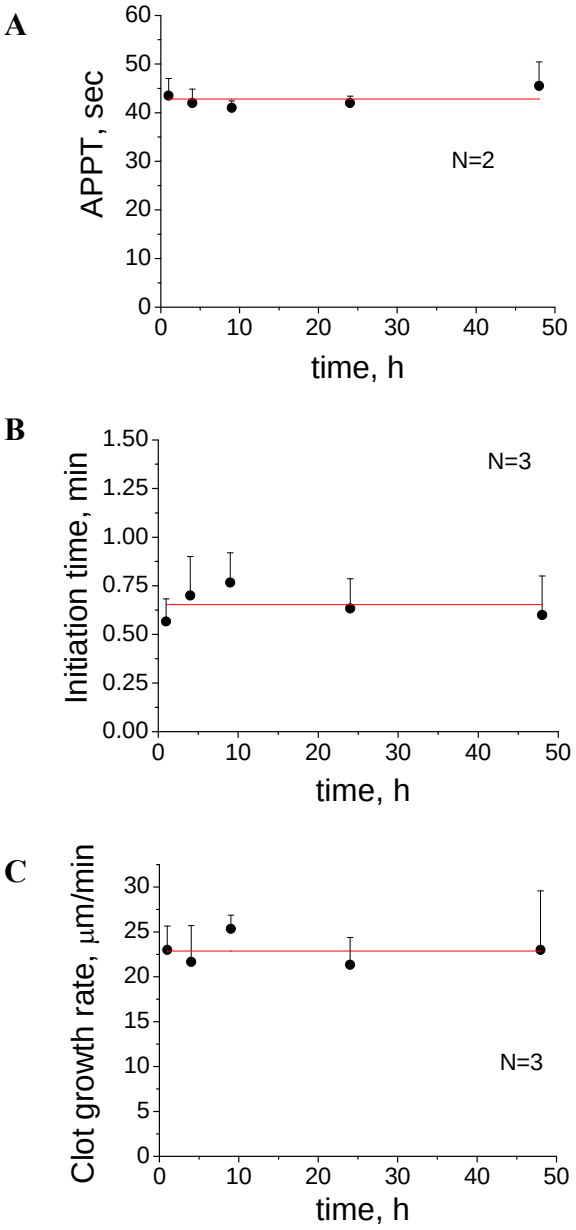
A
APPT, sec
N=2
time, h
B
Initiation time, min
N=3
time, h
C
Clot growth rate, μm/min
N=3
time, h

Fig. S6

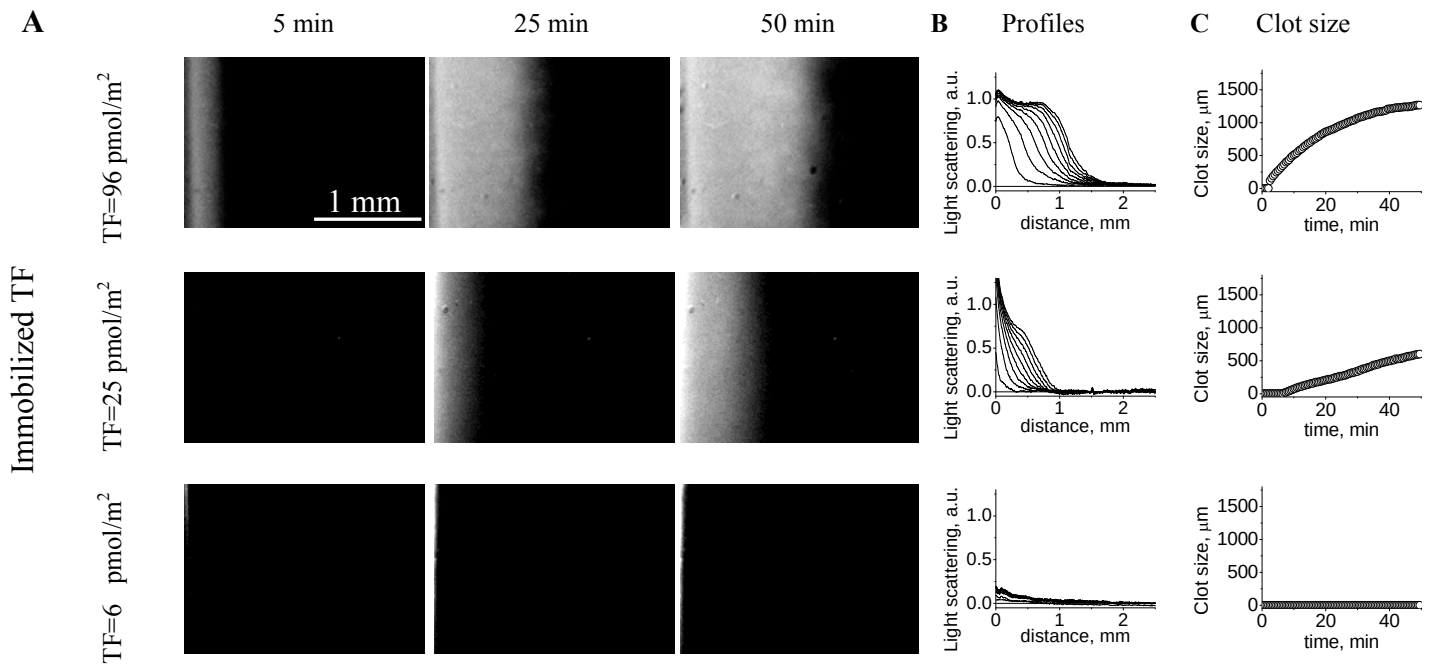
A
5 min
25 min
50 min
B Profiles
C Clot size
Immobilized TF
TF=96 pmol/m2
TF=25 pmol/m2
TF=6 pmol/m2
1 mm
Light scattering, a.u.
distance, mm
Clot size, µm
time, min

Fig. S7

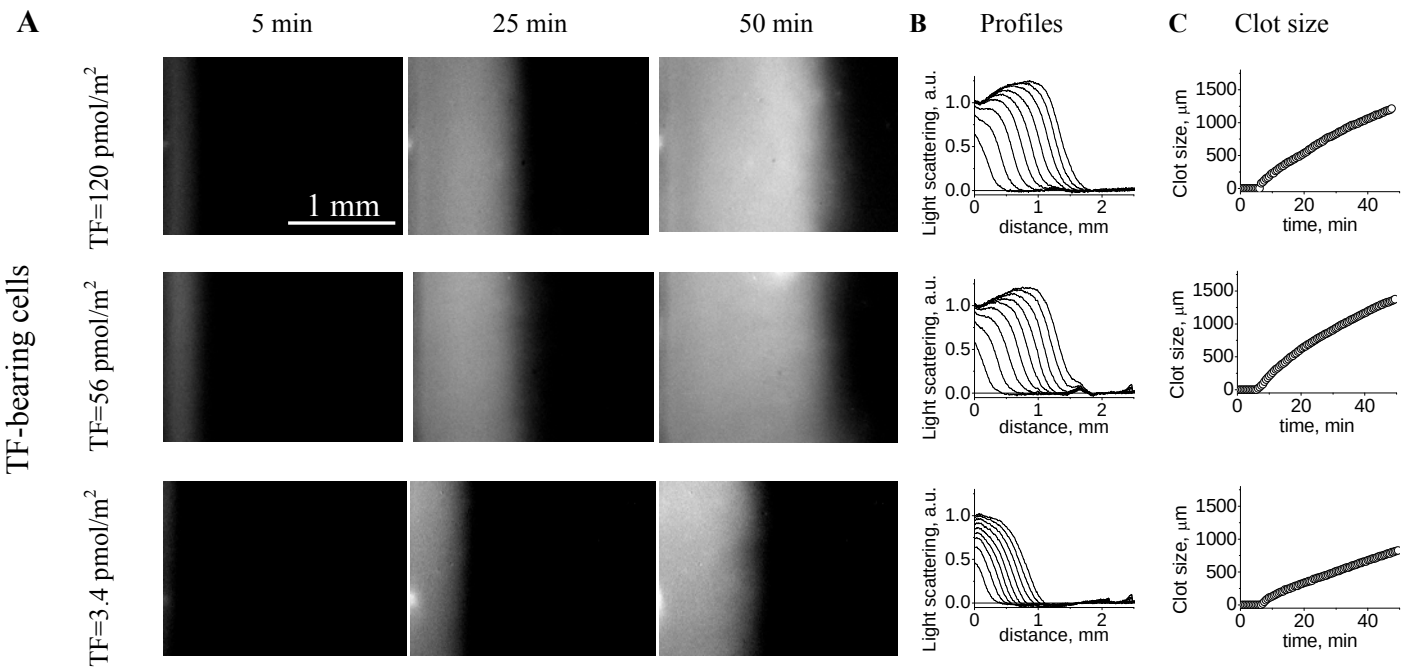
A
5 min
25 min
50 min
B Profiles
C Clot size
TF-bearing cells
TF=120 pmol/m2
TF=56 pmol/m2
TF=3.4 pmol/m2
1 mm
Light scattering, a.u.
distance, mm
Clot size, μm
time, min

Fig. S8

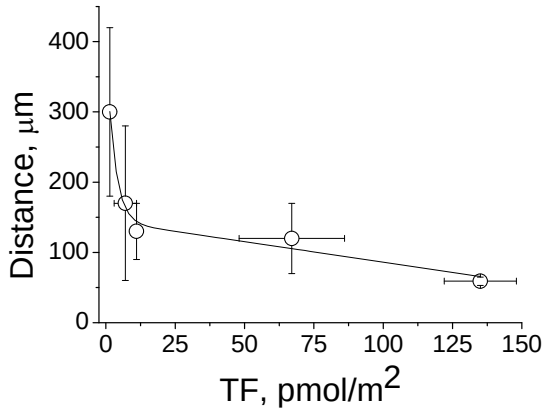

Fig. S9

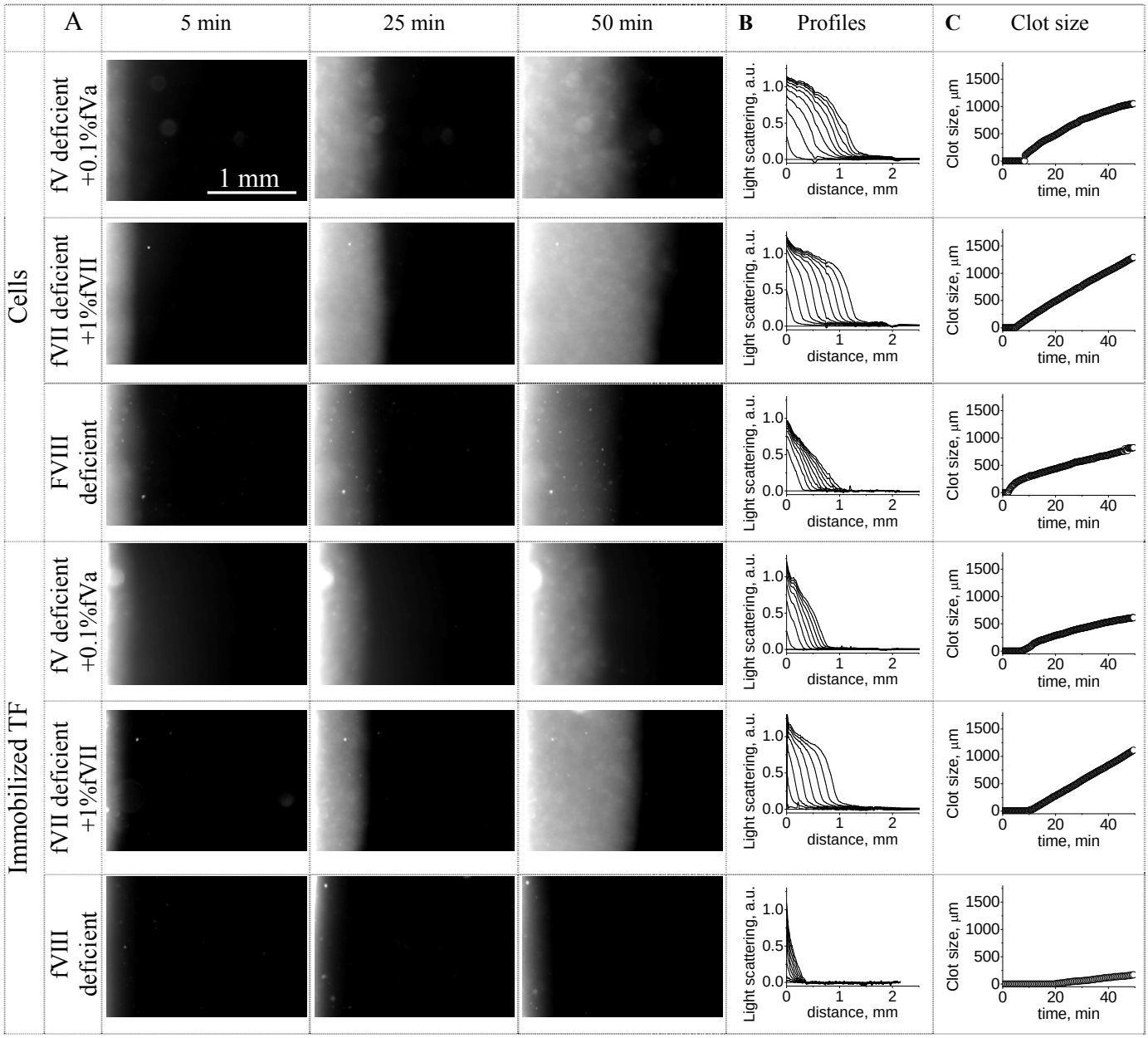
A
5 min
25 min
50 min
B Profiles
C Clot size
Cells
Immobilized TF
fV deficient +0.1%fVa
fVII deficient +1%fVII
FVIII deficient
1 mm
Light scattering, a.u.
distance, mm
Clot size, µm
time, min

Fig. S10

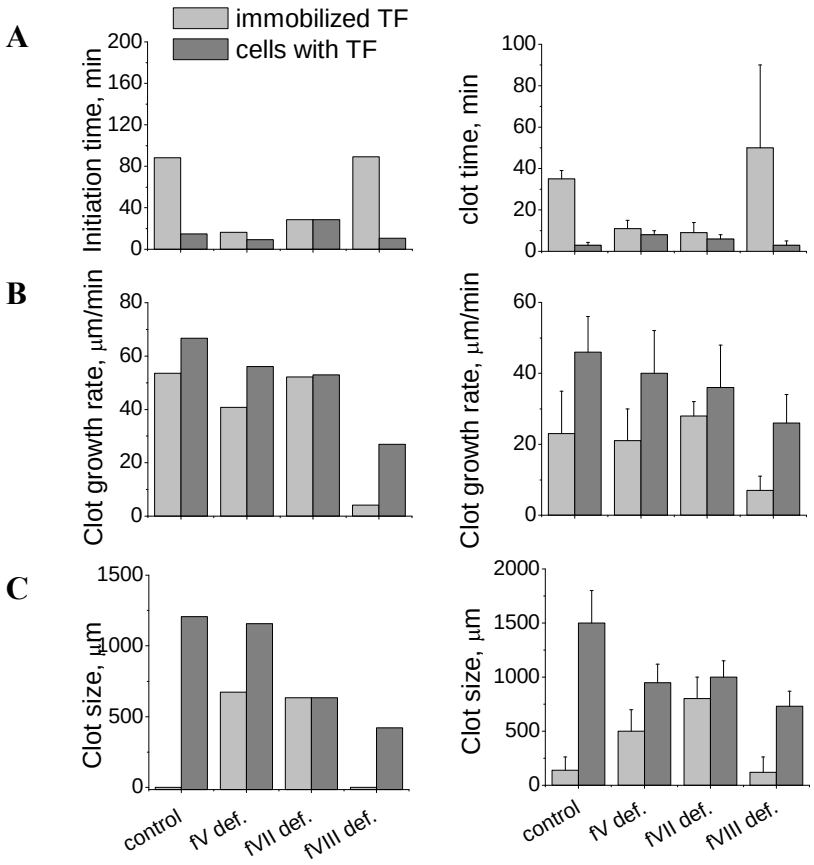
A
B
C
immobilized TF
cells with TF
Initiation time, min
clot time, min
Clot growth rate, μm/min
Clot growth rate, μm/min
Clot size, μm
Clot size, μm
control
fV def.
fVII def.
fVIII def.

Fig. S11

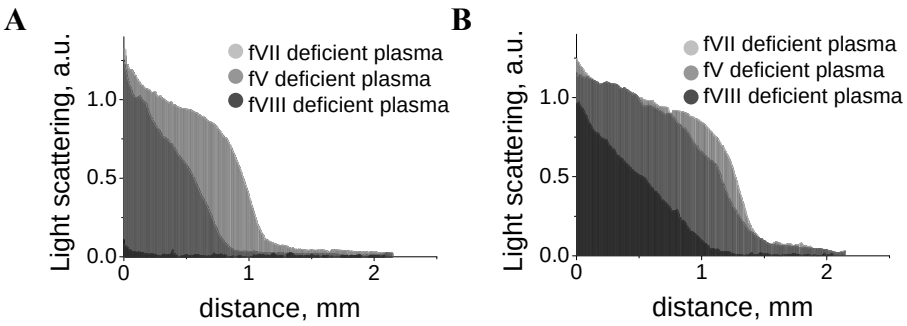
A
B
fVII deficient plasma
fV deficient plasma
fVIII deficient plasma
Light scattering, a.u.
1.0
0.5
0.0
0
1
2
distance, mm